

Improving Text-to-Image Generation with Intrinsic Self-Confidence Rewards

Seungwook Kim¹

Minsu Cho^{1,2}

¹Pohang University of Science and Technology (POSTECH) ²RLWRLD

<https://wookiekim.github.io/SOLACE/>

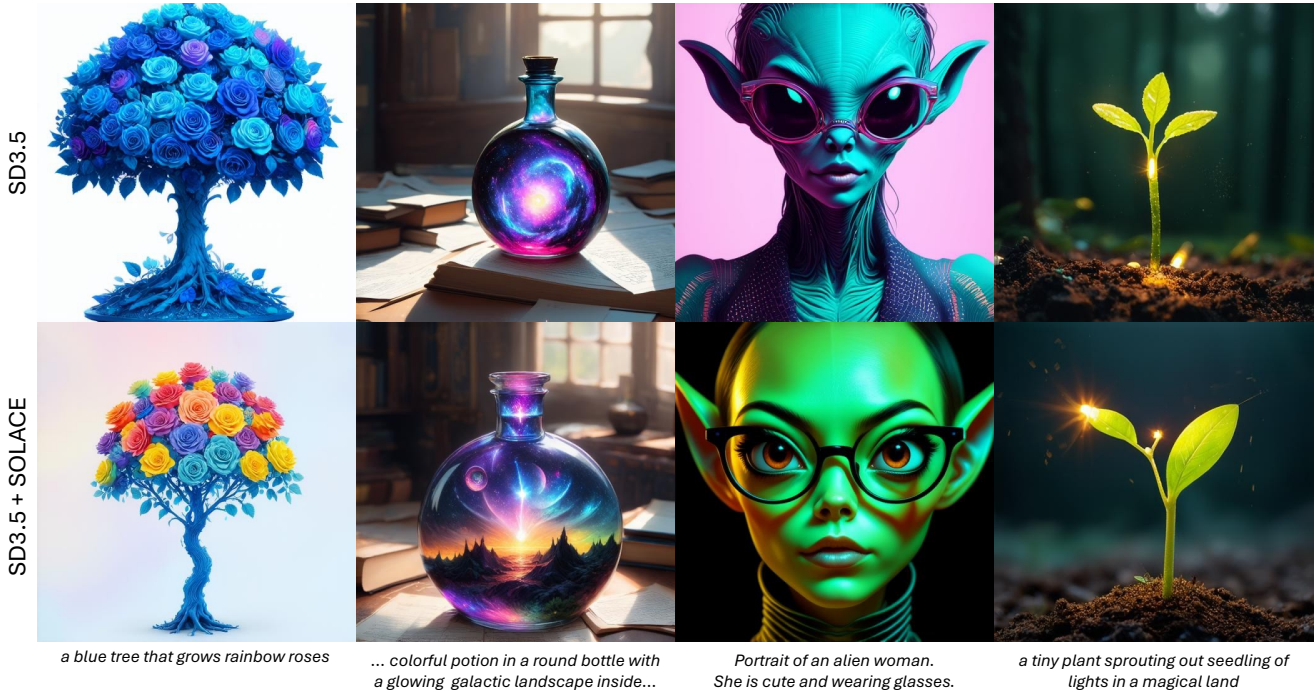


Figure 1. Qualitative examples of SOLACE on Pick-a-Pic dataset [30]. Best viewed on electronics.

Abstract

Text-to-image generation powers content creation across design, media, and data augmentation. Post-training of text-to-image generative models is a promising path to better match human preferences, factuality, and improved aesthetics. We introduce SOLACE (*Self-Originating LATent Confidence Estimation*), a post-training framework that replaces external reward supervision with an internal self-confidence signal, obtained by evaluating how accurately the model recovers injected noise under self-denoising probes. SOLACE converts this intrinsic signal into scalar rewards, enabling fully unsupervised optimization without additional datasets, annotators, or reward models. Empirically, by reinforcing high-confidence generations, SOLACE delivers consistent gains in compositional generation, text rendering and text-image alignment over the baseline. We also find that integrating SOLACE with external rewards results in a complementary improvement, with alleviated reward hacking.

1. Introduction

Text-to-image (T2I) generation has advanced rapidly with the rise of diffusion and flow-based models, delivering high-fidelity, diverse images from natural language prompts [9, 10, 16, 22, 46, 48, 55, 56]. These models now support a broad range of applications: controllable image editing and inpainting [3, 6, 7, 60, 62, 76, 87]; serving as powerful priors or pre-trained components for text-to-video diffusion models [24, 26, 31, 70, 71, 92]; data creation and augmentation pipelines for downstream perception tasks [64, 73, 80]; and text-to-3D (and 4D) reconstruction via score distillation sampling [1, 50, 61, 65, 74]. Recent studies show that *post-training text-to-image generative models* via reinforcement learning can tailor these models to show dramatic improvements in visual appeal and aesthetic quality [5, 36, 69], typically by optimizing external rewards derived from human preference models [30, 75, 78] or task-specific validators [14, 21].

However, defining a scalable and reliable reward for

“good” images remains challenging [30, 33, 67, 75, 78]. There are numerous, weakly-aligned criteria a good image has to satisfy, *e.g.*, compositionality, text rendering, aesthetics, and text–image alignment, whose relative importance shifts across domains and prompts [33]. In practice, external-reward post-training is also vulnerable to over-optimization: optimizing a narrow critic can induce reward hacking and regressions on non-target capabilities, degrading coverage or faithfulness even as the targeted score rises [5, 36, 69]. Human-preference based reward models [30, 72, 78] are popular for their efficacy, but require large-scale annotation for training. Operationally, external rewards require running additional evaluators (preference/OCR/safety models) alongside the generator during training, increasing pipeline complexity.

Despite extensive progress in extrinsically supervised post-training, relying on intrinsic signals remains under-explored for text-to-image generation. In this work, we aim to answer a fundamental question: *can internal feedback from the text-to-image generator itself provide meaningful signals for post-training?* To this end, we introduce Self-Originating Latent Confidence Estimation (SOLACE), a post-training framework that relies on intrinsic self-certainty as the model-native reward. Inspired by Score Distillation Sampling [50, 61, 74], which leverages a pre-trained text-to-image generator as a critic for text-to-3D or -4D generation, we propose to leverage a text-to-image generator to *critique its own generation*. Concretely, given a sampled latent z_0 , we re-noise z_0 to selected timesteps $t \in \mathcal{T}$ using the model’s forward noising schedule, and measure how well the model reconstructs the injected noise, rewarding small residuals as ‘high confidence’. Our hypothesis is that large-scale pretraining in diffusion generative models endows them with priors over real images and text–image alignment, so the model’s self-confidence would align strongly with text-alignment and realism.

Empirically, SOLACE yields consistent gains in compositional generation [21], text rendering [14], and text–image alignment [53], while modestly improving human-preference scores [30, 72, 75, 78] without external rewards. Qualitative side-by-side comparisons and a comprehensive user study corroborate these trends. Together, the results indicate that intrinsic self-confidence aligns with key facets of image generation. Moreover, applying SOLACE on top of an *extrinsically post-trained* model (*i.e.*, using external rewards) recovers additional improvements in compositionality, text rendering, and alignment, with only slight drops on the targeted external metric, evidencing that intrinsic and extrinsic rewards are complementarily beneficial for post-training stronger T2I generators.

The key contributions of our work are as follows:

- We present **SOLACE** (Self-Originating Latent Confidence Estimation), a post-training framework

to use *self-confidence* as a reward for text-to-image generators.

- We define SOLACE’s self-confidence reward by re-noising the model’s own outputs and rewarding accurate recovery of the injected noise - a training-aligned signal that serves as a principled self-confidence score.
- Across standard benchmarks and a comprehensive user study, SOLACE yields consistent gains in compositionality, text rendering, and text–image alignment, while modestly improving human-preference metrics.
- SOLACE complements *external*-reward pipelines: applying SOLACE on top of externally post-trained models improves non-target capabilities (compositionality, text rendering, alignment) with only mild trade-offs on the targeted external metric, mitigating reward hacking.

2. Related Work

Text-to-image generative models. Text-to-image generation is a rapidly advancing field, which was initially dominated by diffusion models [2, 9, 10, 46, 48, 55, 56]. Recent studies tend to focus more on flow matching [3, 16, 63] and sequence models [8, 42, 68, 81] for improved efficiency in train/test time, and enhanced image generation performance. Various innovative techniques are being proposed across architectures [3, 16, 46], image recaptioning [4, 9, 10] and tokenization [29, 68, 82] to further improve the potential of text-to-image generation. In this work, we focus on reinforcement-learning based post-training of text-to-image models to improve a pretrained text-to-image generation model, by using the self-confidence of the generative model as the *intrinsic* reward.

Text-to-image model alignment via post-training. Post-training is emerging as an effective paradigm to align existing text-to-image models to output image to desired directions *e.g.*, human preference. This post-training can take the form of direct fine-tuning given differentiable rewards [13, 51, 52, 78] or Reward Weighted Regression (RWR) [15, 17, 32, 47]. Some post-training schemes build on reinforcement learning to leverage PPO [58]-style policy gradients [5, 18, 25, 44, 89], or perform Direct Preference Optimization (DPO) or its variants [19, 34, 34, 38, 39, 54, 69, 79, 83, 86]. More recently, Flow-GRPO [37] introduces GRPO [59] for flow matching models, by converting the ODE of flow matching sampling to SDEs to inject stochasticity. However, leveraging external rewards results in enhanced costs from having another model during training and also increased risks of reward hacking [38, 39, 54, 69]. In this work, we formulate the self-certainty of text-to-image generated outputs as the ability to recover the noise injected to its own generated outputs, which we leverage as the *intrinsic* signal to perform post-training, resulting in improved text-to-image generation without reward hacking.

Intrinsic signals for post-training. Intrinsic signals for post-training have recently gained traction in language modeling as scalable alternatives to human-labeled preference data, leveraging self-derived feedback such as confidence/uncertainty estimates, self-evaluation, and self-consistency to guide reinforcement learning or preference optimization without annotators [11, 12, 49, 77, 84, 85, 88, 90, 93]. Recently, Inuitior [90] showed that using self-certainty as a confidence-based intrinsic reward enables single-agent reinforcement learning across diverse tasks without relying on explicit feedback, gold labels, or environment-based validation. Bringing the same principle to text-to-image generation is non-trivial: generation proceeds along continuous denoising trajectories and likelihoods are implicit, unlike token-level discrete objectives in LLMs. In this work, we instantiate self-certainty of flow-matching models as their ability to recover the noise injected to its generated outputs, inspired by score-distillation sampling semantics [50, 61]. This enables us to obtain dense, on-policy feedback without additional datasets or reward models. Empirically, we show that this confidence signal aligns with key facets of image generation, i.e., compositionality, text rendering, and text–image alignment.

3. Preliminary: GRPO for Flow Matching

3.1. Flow Matching and Rectified Flow

Flow matching bypasses score learning in conventional diffusion models [27, 66] by directly regressing the target velocity of a transport ODE along a user-chosen path between data and a reference distribution [35, 40]. Recent state-of-the-art generative models [3, 16, 31, 70] adopt the Rectified Flow (RF) framework. Specially, let $x_0 \sim p_{\text{data}}$ and $x_1 \sim p_1$ (e.g., $\mathcal{N}(0, I)$); RF chooses the straight-line path

$$x_t = (1 - t)x_0 + tx_1, \quad (1)$$

for which the target velocity is constant in t :

$$v^* = \partial_t x_t = x_1 - x_0. \quad (2)$$

Training reduces to direct regression of this constant velocity at random (x_t, t) pairs:

$$\mathcal{L}(\theta) = \mathbb{E}_{x_0 \sim p_{\text{data}}, x_1 \sim p_1, t \sim \mathcal{U}(0,1)} \left\| v - v_\theta(x_t, t) \right\|_2^2. \quad (3)$$

After training, sampling solves the deterministic ODE

$$\frac{dx_t}{dt} = v_\theta(x_t, t), \quad t : 1 \rightarrow 0, \quad (4)$$

starting from $x_1 \sim p_1$ and transporting to x_0 .

3.2. GRPO for Flow Matching

For a policy π_θ , we consider a policy-gradient objective that maximizes expected cumulative reward while regularizing updates toward a reference policy π_{ref} via a KL penalty:

$$\max_{\theta} \mathbb{E}_{(s_0, a_0, \dots, s_T, a_T) \sim \pi_\theta} \left[\sum_{t=0}^T R(s_t, a_t) - \beta \sum_{t=0}^T D_{\text{KL}}(\pi_\theta(\cdot | s_t) \| \pi_{\text{ref}}(\cdot | s_t)) \right], \quad (5)$$

where $R(s_t, a_t)$ is the per-step reward. Group Relative Policy Optimization (GRPO) [59] proposes to use a group relative formulation to estimate the advantage for each sample to optimize Eq. (5).

Flow-GRPO [59] proposes to integrate GRPO into flow matching models for online RL post-training. The iterative denoising process in flow matching can be formulated as a Markov Decision Process [5]: given a text prompt c , the flow model p_θ samples a group of G images $\{x_0^i\}_{i=1}^G$ and the corresponding sampling trajectories $\{(x_T^i, x_{T-1}^i, \dots, x_0^i)\}_{i=1}^G$. The advantage of the i -th image is calculated by normalizing the group-level rewards:

$$\hat{A}_t^i = \frac{R(x_0^i, c) - \text{mean}(\{R(x_0^i, c)\}_{i=1}^G)}{\text{std}(\{R(x_0^i, c)\}_{i=1}^G)} \quad (6)$$

Finally, GRPO optimizes the policy model by maximizing $\mathcal{J}_{\text{Flow-GRPO}} = \mathbb{E}_{c \sim C, \{x^i\}_{i=1}^G \sim \pi_{\theta_{\text{old}}}(\cdot | c)} f(r, \hat{A}, \theta, \epsilon, \beta)$, where

$$\begin{aligned} f(r, \hat{A}, \theta, \epsilon, \beta) &= \text{mean}_{i,t} \left[\min(r_t^i, \text{clip}_\epsilon(r_t^i)) \hat{A}_t^i \right] - \beta \bar{D}_{\text{KL}}, \\ \bar{D}_{\text{KL}} &= \text{mean}_t D_{\text{KL}}(\pi_\theta(\cdot | s_t) \| \pi_{\text{ref}}(\cdot | s_t)), \\ \text{clip}_\epsilon(r) &\triangleq \text{clip}(r, 1 - \epsilon, 1 + \epsilon). \end{aligned} \quad (7)$$

and $r_t^i(\theta) = \frac{p_\theta(x_{t-1}^i | x_T^i, c)}{p_{\theta_{\text{old}}}(x_{t-1}^i | x_T^i, c)}$. Flow-GRPO then converts the deterministic ODE of Eq. (4) into an equivalent SDE that matches the original model’s marginal probability function at all timesteps, in order to meet the GRPO policy update requirements, e.g., stochasticity is necessary for increased randomness, which is directly related to “exploration” in RL post-training. We adopt Flow-GRPO in our work to post-train flow-matching based text-to-image generative models.

4. Self-Originating LATent Confidence Estimation

Overview. We present SOLACE (Self-Originating LATent Confidence Estimation), a post-training method for text-to-image generators that eschews reliance on external reward models. SOLACE leverages the model’s own self-confidence as an intrinsic reward: after generating an output, we re-noise it at selected timesteps and score how ac-

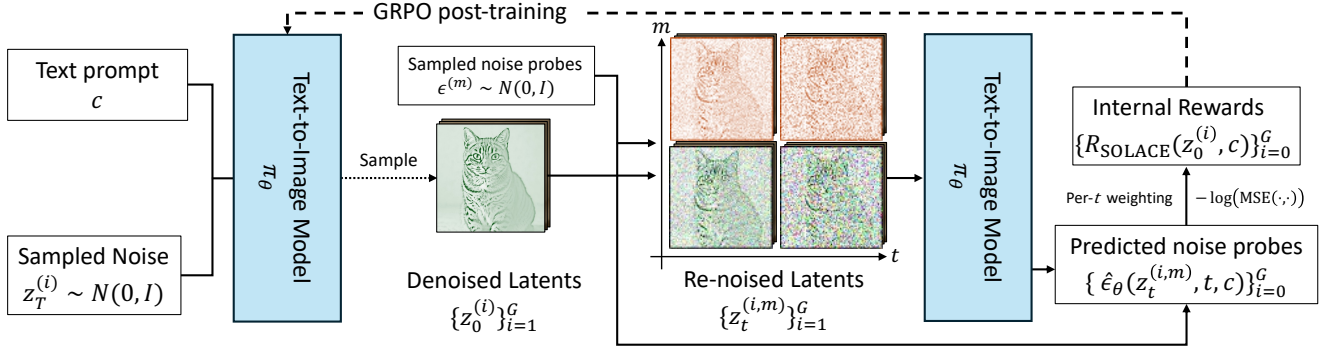


Figure 2. **Overview of SOLACE.** Given a text prompt c , we generate G different latents. Without decoding, we re-noise the latents using K noise probes across $t \in \mathcal{T} \subset [0, 1]$. For each generated latent $z_0^{(i)}$, we formulate the text-to-image generative model’s self-confidence of the generated latent as the ability to denoise the re-noised latent. We leverage this self-confidence as an internal reward scalar value, which we use to post-train the text-to-image generative model using GRPO [37, 59]. We omit the KL term in this figure for better readability.

curately the model recovers the injected noise. Aggregating these per-timestep recovery errors yields a single on-policy scalar reward for reinforcement learning. In the following, we detail the computation of the self-confidence reward (Sec. 4.1), and the stabilization and efficiency techniques used for using SOLACE (Sec. 4.2). An overview of SOLACE is shown in Fig. 2.

4.1. Intrinsic Self-Confidence Reward

Sampling group of images for GRPO. Given a text prompt c , we sample G independent reverse trajectories in the latent space \mathcal{Z} under the flow policy π_θ :

$$z_T^{(i)} \sim \mathcal{N}(0, I), z_{t-1}^{(i)} \sim \pi_\theta(\cdot | z_t^{(i)}, c), i = 1, \dots, G. \quad (8)$$

This produces terminal latents $\{z_0^{(i)}\}_{i=1}^G$ and trajectories $\{(z_T^{(i)}, z_{T-1}^{(i)}, \dots, z_0^{(i)})\}_{i=1}^G$. Using multiple independent draws yields the group required for group-relative advantage normalization in GRPO. While we can sample G different images from the same initial noise z_T due to the added stochasticity from [37], we sample different initial noise for improved exploration for efficient GRPO training.

Sampling noise probes for re-noising. We draw a shared set of K noise probes in latent space:

$$\epsilon^{(m)} \sim \mathcal{N}(0, I), \quad m = 1, \dots, K, \quad (9)$$

so that candidate i and candidate j are perturbed by the *same* probes $\{\epsilon^{(m)}\}_{m=1}^K$. For rectified flow, we re-noise a terminal latent $z_0^{(i)}$ via the linear forward kernel

$$z_t^{(i,m)} = (1-t)z_0^{(i)} + t\epsilon^{(m)}, \quad t \in \mathcal{T} \subset [0, 1], \quad (10)$$

where \mathcal{T} is the set of re-noising levels used for evaluation. We take K even ($K \geq 2$) and use antithetic pairing to enforce exact mean zero within the probe set, i.e., $\epsilon^{(m+K/2)} = -\epsilon^{(m)}$ for $m = 1, \dots, K/2$.

Calculating self-confidence. For each noised latent $z_t^{(i,m)}$ (Eq. (10)), we query the flow-matching model’s velocity field $v_\theta(z_t^{(i,m)}, t, c)$. Under the rectified-flow parameterization, the velocity predicts a linear transform of the injected noise; specifically, we recover a noise estimate via

$$\hat{\epsilon}_\theta(z_t^{(i,m)}, t, c) = v_\theta(z_t^{(i,m)}, t, c) + z_0^{(i)}. \quad (11)$$

We then measure the reconstruction error against $\epsilon^{(m)}$:

$$\text{MSE}_{i,t} = \frac{1}{K} \sum_{m=1}^K \left\| \hat{\epsilon}_\theta(z_t^{(i,m)}, t, c) - \epsilon^{(m)} \right\|_2^2. \quad (12)$$

To turn small errors into large rewards while stabilizing dynamic range, we use the negative log transform,

$$S_{i,t} = -\log(\text{MSE}_{i,t} + \delta), \quad (13)$$

where $\delta > 0$ avoids $\log 0$. This choice (i) approximates a Gaussian log-likelihood score under an i.i.d. noise model, (ii) compresses outliers, and (iii) yields additive contributions across timesteps. Aggregating over a set of re-noising levels $\mathcal{T} \subset [0, 1]$ gives the scalar intrinsic reward

$$R_{\text{SOLACE}}(z_0^{(i)}, c) = \frac{1}{\sum_{t \in \mathcal{T}} w(t)} \sum_{t \in \mathcal{T}} w(t) S_{i,t}. \quad (14)$$

We use $w(t) = 1$ in practice for simplicity. Note that external rewards typically operate in pixel space, $R_{\text{ext}}(x^{(i)}, c)$, where $x^{(i)} = \text{Dec}(z_0^{(i)})$ for a fixed decoder $\text{Dec}: \mathcal{Z} \rightarrow \mathcal{X}$. In contrast, R_{SOLACE} is computed *directly in latent space*, avoiding decoding and keeping the signal model-native.

4.2. Stabilization and Efficiency Techniques

Denosing reduction for efficient training. Following Flow-GRPO [37], we shorten the reverse-time horizon during training by subsampling the denoising steps. This reduces compute without degrading downstream gains: e.g.,

while SD3.5 uses 40 sampling steps at inference, we use 10 denoising steps during training. We empirically find that this does not sacrifice image quality at test time, but facilitates substantially faster training.

Timestep selection for self-confidence probing. We probe self-confidence at the *exact scheduler timesteps* used by the SD3.5 sampler (same discretization and indices), ensuring the suffix window align with the generation trajectory. This on-policy, solver-aware choice avoids distributional mismatch between sampling and self-confidence probing, yielding more reliable credit assignment across steps.

Training on selective timesteps. We observed that using all training denoising trajectories easily leads to collapse (e.g., blank / textureless images), a form of reward hacking in which the model steers latents toward regimes that make injected noise overly easy to predict. We mitigate this by optimizing the sampled trajectories from only a suffix of the training schedule, i.e., a fixed percentage of the later reverse steps, where the denoising task remains informative but less exploitable. Let $\mathcal{T}_{\text{train}} \subset \mathcal{T}$ denote this suffix window ($|\mathcal{T}_{\text{train}}| = \lceil \rho |\mathcal{T}| \rceil$); we apply GRPO losses only on $t \in \mathcal{T}_{\text{train}}$, which stabilizes learning without collapse.

Self-Confidence calculation with CFG. Although G images are sampled with CFG for GRPO training, our SOLACE self-confidence is computed *without* CFG. CFG forms a mixture field $v_{\text{cfg}} = v_{\text{uncond}} + s(v_{\text{cond}} - v_{\text{uncond}})$; this mixture would calculate a self-certainty based on the guided proxy rather than the base conditional model trained on data. In our experiments, omitting CFG during self-confidence computation yields stronger and more stable improvements.

Online calculation of self-confidence. When computing self-confidence for SOLACE, we can either compute it (1) online, using the model being trained (π_θ), or (2) offline, using a fixed based model (π_{ref}) for the self-confidence calculation. While we do not observe severe over-optimization [20] when computing the self-confidence in an offline manner, we notice that the performance improves when we compute self-confidence rewards in an online manner. We conjecture that as the model improves through SOLACE post-training, the stability and reliability of self-confidence improves as well, leading to a stronger improvement in performance.

5. Experiments

5.1. Implementation details

We use a group size $G = 16$ and number of noise probes $K = 8$ with antithetic pairing in our experiments. While we do not need external reward models for training, we still need text prompts to generate the terminal latents for training; we use the train set of the visual text rendering

task [14] from Flow-GRPO [37], which holds longer and more informative prompts compared to Pick-a-Pic [30] or GenEval [21]. We use parameter-efficient post-training via leveraging LoRA [28, 43] with rank $r = 32$ and scaling factor $\alpha = 64$. We use the AdamW [41] optimizer with constant learning rate of $3e^{-4}$, and the KL regularizer weight $\beta = 0.04$. In $|\mathcal{T}_{\text{train}}| = \lceil \rho |\mathcal{T}| \rceil$, we set $\rho = 0.6$, which we find to show improvements without reward hacking or training collapse. An image resolution of 512×512 is used for both training and testing. We use CFG guidance of 7.0 at inference. All experiments are carried out on $8 \times$ NVIDIA RTX PRO 6000 Blackwell GPUs. We include more training details in the supplementary materials.

5.2. Evaluation setting

(1) Compositional image generation. We evaluate on GenEval [21] that consists of complex compositional prompts including object counting, attribute bounding or spatial relations. Evaluation is performed across six tasks of position, counting, attribute binding, colors, two objects, and single object. We adhere to the official evaluation pipeline to detect object bounding boxes and colors, then infers their spatial relations, when given a generated image. The rewards are then calculated in a rule-based manner e.g. for object counting, $r = 1 - \frac{|N_{\text{gen}} - N_{\text{ref}}|}{N_{\text{ref}}}$, where N_{gen} is the number of generated objects, while N_{ref} is the specified number of objects in the prompt.

(2) Visual text rendering. We use the 1,000 GPT4o [45]-generated test prompts from [37]. In each prompt, the exact string that should appear in the image (i.e. target text) is specified by " $\{\text{t}_{\text{text}}\}$ ". We adhere to [22] to report $r = \max(0, 1 - \frac{N_e}{N_{\text{ref}}})$, where N_e is the minimum edit distance between the rendered text and the target text, and N_{ref} is the non-whitespace length of the target text.

(3) Human preference alignment. We report the model-based reward outputs from Pickscore [30], HPSv2 [75], ImageReward [78] and UnifiedReward [72], which are models trained with large-scale human annotated preference data. We use the test prompts from DrawBench [56] to generate the images for evaluation.

(4) Image quality evaluation. We additionally report the CLIP-Score [53] and Aesthetic Score [57] on DrawBench [56], to evaluate the overall quality of generated images independent of the above task-specific criteria.

5.3. Results

Quantitative results. The evaluation results are shown in Tab. 1, where it can be seen that applying our proposed SOLACE on the T2I flow-matching model SD3.5-M for post-training yields consistent gains across task-specific, image quality, and human preference metrics. While improvements in human preference is modest, we observe

Model	Task-specific		Image Quality		Human Preference			
	GenEval	OCR	ClipScore	Aesthetic	PickScore	HPSv2.1	ImageReward	UnifiedReward
SD-XL	0.55	0.14	0.287	5.60	22.42	0.280	0.76	2.93
SD3.5-L	0.71	0.68	0.289	5.50	22.91	0.288	0.96	3.25
SD3.5-M	0.65	0.61	0.282	5.36	22.34	0.279	0.84	3.08
+ SOLACE (Ours)	0.71	0.67	0.288	5.39	22.41	0.278	0.87	3.11
SD3.5-M	0.95	0.65	0.293	5.32	22.51	0.272	1.06	3.18
+ FlowGRPO	0.67	0.92	0.290	5.32	22.41	0.280	0.95	3.14
	0.54	0.68	0.278	5.90	23.50	0.314	1.26	3.37
SD3.5-M	0.92	0.71	0.294	5.35	22.50	0.277	1.06	3.26
+ FlowGRPO	0.72	0.89	0.291	5.39	22.45	0.284	0.97	3.19
+SOLACE (Ours)	0.77	0.70	0.287	5.63	22.73	0.286	1.07	3.26

Table 1. **Quantitative results of SOLACE.** We evaluate SOLACE post-training on base models of SD3.5 [16], on GenEval [21], Text Rendering, human preference reward models [30, 72, 75, 78], and image quality metrics. We show that SOLACE post-training yields consistent gains across text-to-image generative models on different quantitative metrics.

PartiPrompts			HPSv2		
SD3.5 + SOLACE (59.0%)	Same (14.5%)	SD3.5-M (26.5%)	SD3.5 + SOLACE (50.6%)	Same (24.4%)	SD3.5-M (25.0%)
<i>Which image is more visually realistic and appealing?</i>					
SD3.5 + SOLACE (57.3%)	Same (28.4%)	SD3.5-M (14.3%)	SD3.5 + SOLACE (40.6%)	Same (40.6%)	Same (18.8%)
<i>Which image better aligns with the text description?</i>					

Figure 3. **User study against baseline SD3.5-M [16] on PartiPrompts [56] and HPSv2 [75].** The user study shows that SOLACE post-training yields favorable visual realism/appeal, and text-image alignment.

a considerable improvement in performance on compositional generation (GenEval [21]), text rendering (OCR[14]) and CLIPScore [53], almost matching the performance of SD3.5-L in these three metrics, albeit having less than $\frac{1}{3}$ of the parameters (2.5B vs. 7.1B). This evidences that the text-to-image generative model’s intrinsic confidence is strongly correlated with the success of compositional generation, text rendering and text-image alignment, which are more objective metrics compared to human preferences.

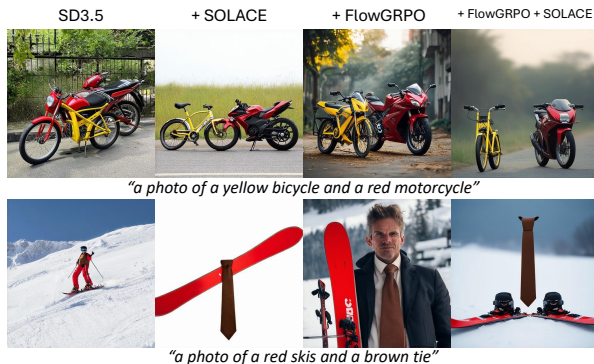


Figure 4. **Effect of SOLACE post-training SD3.5-M after post-training on PickScore [30] using FlowGRPO [37].** SOLACE complements external rewards, showing the best best compositional generation and visual appeal on GenEval [21]. Post-training on external rewards yields high visual appeal, but sacrifices compositionality as shown above (Column 3: Generates yellow motorcycle instead / generates unwanted human).

We also analyze the effect of applying SOLACE post-training *after* post-training SD3.5-M on external rewards using Flow-GRPO [37]. The results show that while the performance on the external reward itself is mildly compromised, we consistently gain noticeable improvements across GenEval, OCR and CLIPScore, which strengthens our hypothesis that the intrinsic confidence of text-to-image generative model is strongly correlated with the success of compositional generation, text rendering and text-image alignment. In Fig. 4, we provide visual examples of SD3.5-M post-trained with FlowGRPO using PickScore as the external reward, finally post-trained with SOLACE intrinsic self-certainty rewards. It shows that integrating SOLACE improves the generative performances even further, evidencing the complementarity of SOLACE and external rewards.

User study. In Fig. 3, we provide the results of a user study on prompts from PartiPrompt [81] and HPSv2 [75], asking users to assess the generated images based on visual appeal/realism and text alignment. We summarize $\sim 1,800$ responses from 20 participants. The user study results show that applying SOLACE post-training SD3.5-M consistently outperforms the baseline model in terms of visual realism/appeal and text alignment.

Qualitative comparison. We provide additional qualitative comparisons in Fig. 1 and Fig. 5, where it can be seen that

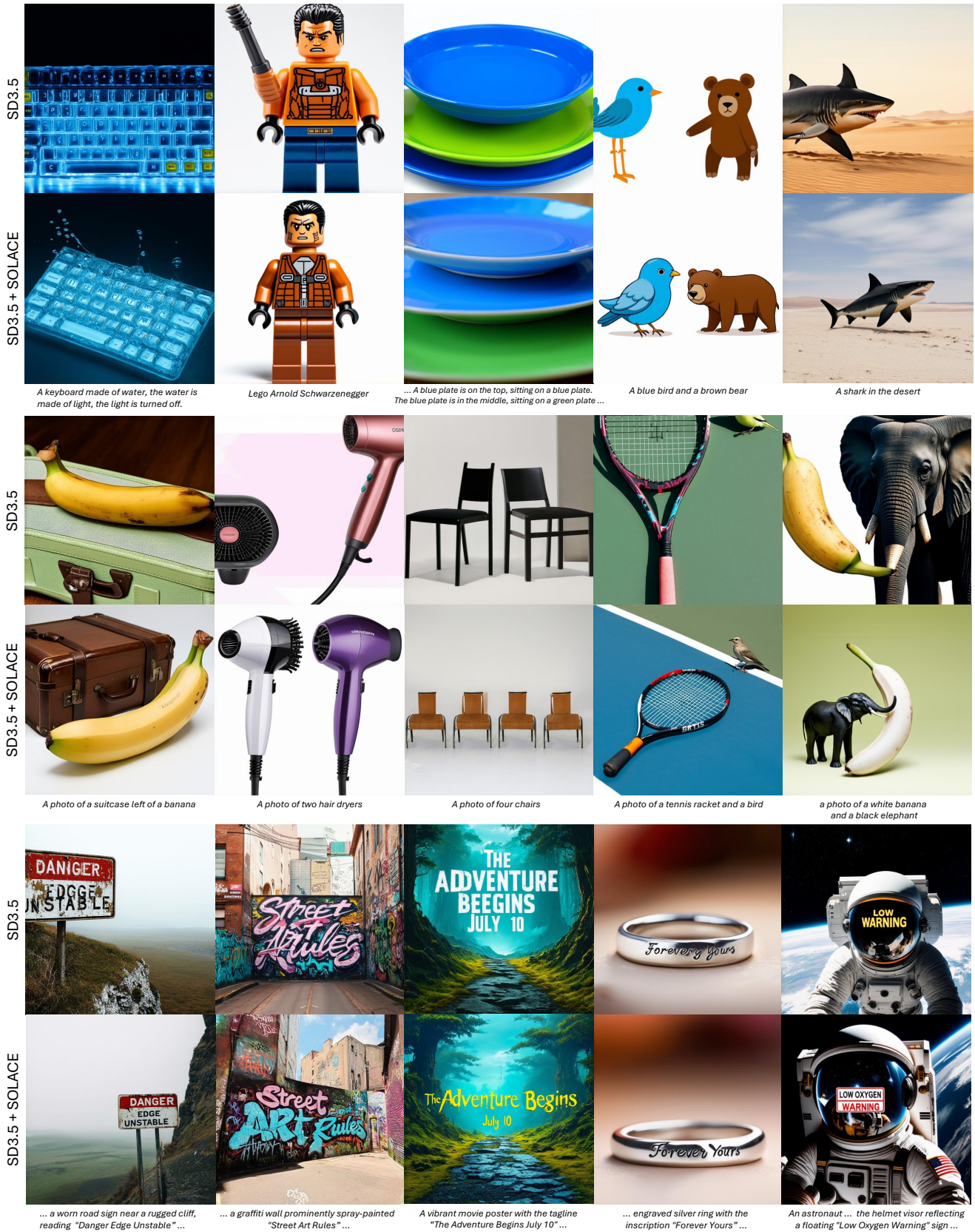


Figure 5. Qualitative results of SOLACE when applied on SD3.5 [16] on DrawBench [56], GenEval [21] and OCR [14]. It can be seen that applying SOLACE shows consistent improvements over the baseline SD3.5.

	Task-specific		Image Quality		Human Preference			
	GenEval	OCR	ClipScore	Aesthetic	PickScore	HPSv2.1	ImageReward	UnifiedReward
<i>Number of noise probes K</i>								
$K = 4$	0.71	0.66	0.287	5.37	22.34	0.273	0.81	3.08
$K = 8$ (Ours)	0.71	0.67	0.288	5.39	22.41	0.278	0.87	3.11
$K = 16$	0.70	0.67	0.288	5.42	22.34	0.278	0.86	3.09
<i>Classifier-Free Guidance for self-confidence calculation</i>								
O	0.68	0.59	0.287	5.38	22.39	0.278	0.85	3.10
X (Ours)	0.71	0.67	0.288	5.39	22.41	0.278	0.87	3.11
<i>Offline vs Online Self-Confidence</i>								
Offline	0.69	0.61	0.285	5.36	22.36	0.274	0.82	3.07
Online (Ours)	0.71	0.67	0.288	5.39	22.41	0.278	0.87	3.11

Table 2. **Ablation study results of SOLACE.** We validate the design choices of SOLACE over number of noise probes K , the usage of CFG for self-confidence calculation, and online/offline self-confidence calculation. Our current configurations yield superior results.

applying SOLACE yields visually pleasurable results with improved compositionality and text rendering capabilities, even when trained with no external reward at all.

5.4. Ablation study and analyses

In Tab. 2, we provide ablation study results to validate the design and hyperparameter choices of SOLACE.

Analyses on number of noise probes K . We vary K across 4, 8, 16 - the results show that while mostly similar, $K = 8$ yields slightly better results overall. Although using $K = 16$ outperforms $K = 8$ in terms of aesthetic score, we decided that this improvement is negligible in comparison to the additional computation overhead during training.

CFG for self-confidence. We show that using CFG during self-confidence computation at post-training results in a slight drop in the overall performance. We conjecture this is because CFG itself is an inference-time technique, and using CFG inside the reward would optimize the *guided proxy* rather than the base conditional policy $\pi_\theta(\cdot | z_t, c)$. This may incentivize reward hacking via larger guidance strength (larger than 1.0) instead of learning a better π_θ .

Online self-confidence vs Offline self-confidence. We compare the post-training performance when the intrinsic reward is computed in an online manner i.e., calculated using the text-to-image model being trained π_θ , and when computed in an offline manner i.e., calculated using the base model π_{ref} . The results show that using offline self-certainty as a static reward results in a performance drop across performance metrics, hinting that static self-confidence reward is suboptimal in comparison to using online self-certainty.

Observed causes of training collapse. We observe that the training collapses when (1) we train on a higher number of sampling timesteps i.e., $\rho > 0.6$ in $|\mathcal{T}_{\text{train}}| = \lceil \rho |\mathcal{T}| \rceil$, and (2) when we do not use CFG for sampling the G candidates.

We observe that under the two aforementioned cases, over-optimization against the intrinsic self-confidence reward occurs, resulting in textureless images being generated due to severe reward hacking and train collapse. We guide the authors to the supplementary for more details.

5.5. Limitations of SOLACE

One limitation is that the intrinsic self-confidence does not align strongly with human preference, where observed gains are modest. Also, while SOLACE shows to improve compositional generation, text rendering and text faithfulness, we cannot target a specific alignment objective using SOLACE alone. However, we showed that SOLACE can be integrated with external rewards to target specific alignments while alleviating reward hacking and improving compositionality or text rendering capabilities (Tab. 1).

6. Conclusion

We introduced SOLACE, a reinforcement-learning post-training framework that replaces external critics with an intrinsic self-confidence signals. SOLACE converts this self-confidence into stable scalar rewards and optimizes a flow-matching text-to-image generator without auxiliary annotators or task-specific validators. Across benchmarks and a user study, SOLACE yields consistent improvements in compositionality, text rendering and text alignment; a comprehensive user study supports our findings. We also showed that SOLACE can be integrated with external rewards to align text-to-image generation to specific external criteria with mitigated reward hacking and additional improvements. Future directions include (i) consistency-aware extensions (temporal/multi-view) to carry SOLACE to video and 3D generation, and (ii) disentangling and calibrating intrinsic signals to enable precise, task-targeted reward shaping.

Acknowledgement. This work was supported by the IITP grants (RS-2022-II220290: Visual Intelligence for Space-Time Understanding and Generation based on Multi-layered Visual Common Sense (40%), RS-2022-II220113: Developing a Sustainable Collaborative Multi-modal Lifelong Learning Framework (50%), RS-2019-II191906: AI Graduate School Program at POSTECH (5%), RS-2025-02653113: High-Performance Research AI Computing Infrastructure Support at the 2 PFLOPS Scale (5%)) funded by the Korea government (MSIT).

References

- [1] Sherwin Bahmani, Ivan Skorokhodov, Victor Rong, Gordon Wetzstein, Leonidas Guibas, Peter Wonka, Sergey Tulyakov, Jeong Joon Park, Andrea Tagliasacchi, and David B Lindell. 4d-fy: Text-to-4d generation using hybrid score distillation sampling. In *Proceedings of the IEEE/CVF Conference on Computer Vision and Pattern Recognition*, pages 7996–8006, 2024. 1
- [2] Fan Bao, Shen Nie, Kaiwen Xue, Yue Cao, Chongxuan Li, Hang Su, and Jun Zhu. All are worth words: A vit backbone for diffusion models. In *Proceedings of the IEEE/CVF conference on computer vision and pattern recognition*, pages 22669–22679, 2023. 2
- [3] Stephen Batifol, Andreas Blattmann, Frederic Boesel, Saksham Consul, Cyril Diagne, Tim Dockhorn, Jack English, Zion English, Patrick Esser, Sumith Kulal, et al. Flux. 1 kontext: Flow matching for in-context image generation and editing in latent space. *arXiv e-prints*, pages arXiv–2506, 2025. 1, 2, 3, 7
- [4] James Betker, Gabriel Goh, Li Jing, Tim Brooks, Jianfeng Wang, Linjie Li, Long Ouyang, Juntang Zhuang, Joyce Lee, Yufei Guo, et al. Improving image generation with better captions. *Computer Science*. <https://cdn.openai.com/papers/dall-e-3.pdf>, 2(3):8, 2023. 2
- [5] Kevin Black, Michael Janner, Yilun Du, Ilya Kostrikov, and Sergey Levine. Training diffusion models with reinforcement learning. *arXiv preprint arXiv:2305.13301*, 2023. 1, 2, 3
- [6] Frederic Boesel and Robin Rombach. Improving image editing models with generative data refinement. In *The Second Tiny Papers Track at ICLR 2024*, 2024. 1
- [7] Tim Brooks, Aleksander Holynski, and Alexei A Efros. Instructpix2pix: Learning to follow image editing instructions. In *Proceedings of the IEEE/CVF conference on computer vision and pattern recognition*, pages 18392–18402, 2023. 1
- [8] Huiwen Chang, Han Zhang, Jarred Barber, AJ Maschinot, Jose Lezama, Lu Jiang, Ming-Hsuan Yang, Kevin Murphy, William T Freeman, Michael Rubinstein, et al. Muse: Text-to-image generation via masked generative transformers. *arXiv preprint arXiv:2301.00704*, 2023. 2
- [9] Junsong Chen, Jincheng Yu, Chongjian Ge, Lewei Yao, Enze Xie, Yue Wu, Zhongdao Wang, James Kwok, Ping Luo, Huchuan Lu, et al. Pixart- α : Fast training of diffusion transformer for photorealistic text-to-image synthesis. *arXiv preprint arXiv:2310.00426*, 2023. 1, 2
- [10] Junsong Chen, Chongjian Ge, Enze Xie, Yue Wu, Lewei Yao, Xiaozhe Ren, Zhongdao Wang, Ping Luo, Huchuan Lu, and Zhenguo Li. Pixart- σ : Weak-to-strong training of diffusion transformer for 4k text-to-image generation. In *European Conference on Computer Vision*, pages 74–91. Springer, 2024. 1, 2
- [11] Zixiang Chen, Yihe Deng, Huizhuo Yuan, Kaixuan Ji, and Quanquan Gu. Self-play fine-tuning converts weak language models to strong language models. *arXiv preprint arXiv:2401.01335*, 2024. 3
- [12] Pengyu Cheng, Yong Dai, Tianhao Hu, Han Xu, Zhisong Zhang, Lei Han, Nan Du, and Xiaolong Li. Self-playing adversarial language game enhances llm reasoning. *Advances in Neural Information Processing Systems*, 37:126515–126543, 2024. 3
- [13] Kevin Clark, Paul Vicol, Kevin Swersky, and David J Fleet. Directly fine-tuning diffusion models on differentiable rewards. *arXiv preprint arXiv:2309.17400*, 2023. 2
- [14] Cheng Cui, Ting Sun, Manhui Lin, Tingquan Gao, Yubo Zhang, Jiaxuan Liu, Xueqing Wang, Zelun Zhang, Changda Zhou, Hongen Liu, et al. Paddleocr 3.0 technical report. *arXiv preprint arXiv:2507.05595*, 2025. 1, 2, 5, 6, 7
- [15] Hanze Dong, Wei Xiong, Deepanshu Goyal, Yihan Zhang, Winnie Chow, Rui Pan, Shizhe Diao, Jipeng Zhang, Kashun Shum, and Tong Zhang. Raft: Reward ranked finetuning for generative foundation model alignment. *arXiv preprint arXiv:2304.06767*, 2023. 2
- [16] Patrick Esser, Sumith Kulal, Andreas Blattmann, Rahim Entezari, Jonas Müller, Harry Saini, Yam Levi, Dominik Lorenz, Axel Sauer, Frederic Boesel, et al. Scaling rectified flow transformers for high-resolution image synthesis. In *Forty-first international conference on machine learning*, 2024. 1, 2, 3, 6, 7
- [17] Jiajun Fan, Shuaike Shen, Chaoran Cheng, Yuxin Chen, Chumeng Liang, and Ge Liu. Online reward-weighted fine-tuning of flow matching with wasserstein regularization. In *The Thirteenth International Conference on Learning Representations*, 2025. 2
- [18] Ying Fan, Olivia Watkins, Yuqing Du, Hao Liu, Moonkyung Ryu, Craig Boutilier, Pieter Abbeel, Mohammad Ghavamzadeh, Kangwook Lee, and Kimin Lee. Reinforcement learning for fine-tuning text-to-image diffusion models. In *Thirty-seventh Conference on Neural Information Processing Systems (NeurIPS) 2023*. Neural Information Processing Systems Foundation, 2023. 2
- [19] Hiroki Furuta, Heiga Zen, Dale Schuurmans, Aleksandra Faust, Yutaka Matsuo, Percy Liang, and Sherry Yang. Improving dynamic object interactions in text-to-video generation with ai feedback. *arXiv preprint arXiv:2412.02617*, 2024. 2
- [20] Leo Gao, John Schulman, and Jacob Hilton. Scaling laws for reward model overoptimization. In *International Conference on Machine Learning*, pages 10835–10866. PMLR, 2023. 5
- [21] Dhruva Ghosh, Hannaneh Hajishirzi, and Ludwig Schmidt. Geneval: An object-focused framework for evaluating text-to-image alignment. *Advances in Neural Information Processing Systems*, 36:52132–52152, 2023. 1, 2, 5, 6, 7
- [22] Lixue Gong, Xiaoxia Hou, Fanshi Li, Liang Li, Xiaochen Lian, Fei Liu, Liyang Liu, Wei Liu, Wei Lu, Yichun

- Shi, et al. Seedream 2.0: A native chinese-english bilingual image generation foundation model. *arXiv preprint arXiv:2503.07703*, 2025. 1, 5
- [23] Sylvain Gugger, Lysandre Debut, Thomas Wolf, Philipp Schmid, Zachary Mueller, Sourab Mangrulkar, Marc Sun, and Benjamin Bossan. Accelerate: Training and inference at scale made simple, efficient and adaptable. <https://github.com/huggingface/accelerate>, 2022. 3
- [24] Yuwei Guo, Ceyuan Yang, Anyi Rao, Zhengyang Liang, Yaohui Wang, Yu Qiao, Maneesh Agrawala, Dahua Lin, and Bo Dai. Animatediff: Animate your personalized text-to-image diffusion models without specific tuning. *arXiv preprint arXiv:2307.04725*, 2023. 1
- [25] Shashank Gupta, Chaitanya Ahuja, Tsung-Yu Lin, Sreya Dutta Roy, Harrie Oosterhuis, Maarten de Rijke, and Satya Narayan Shukla. A simple and effective reinforcement learning method for text-to-image diffusion fine-tuning. *arXiv preprint arXiv:2503.00897*, 2025. 2
- [26] Yoav HaCohen, Nisan Chiprut, Benny Brazowski, Daniel Shalem, Dudu Moshe, Eitan Richardson, Eran Levin, Guy Shiran, Nir Zabari, Ori Gordon, et al. Ltx-video: Realtime video latent diffusion. *arXiv preprint arXiv:2501.00103*, 2024. 1
- [27] Jonathan Ho, Ajay Jain, and Pieter Abbeel. Denoising diffusion probabilistic models. *Advances in neural information processing systems*, 33:6840–6851, 2020. 3
- [28] Edward J Hu, Yelong Shen, Phillip Wallis, Zeyuan Allen-Zhu, Yuanzhi Li, Shean Wang, Lu Wang, Weizhu Chen, et al. Lora: Low-rank adaptation of large language models. *ICLR*, 1(2):3, 2022. 5
- [29] Dongwon Kim, Ju He, Qihang Yu, Chenglin Yang, Xiaohui Shen, Suha Kwak, and Liang-Chieh Chen. Democratizing text-to-image masked generative models with compact text-aware one-dimensional tokens. *arXiv preprint arXiv:2501.07730*, 2025. 2
- [30] Yuval Kirstain, Adam Polyak, Uriel Singer, Shahbuland Matiana, Joe Penna, and Omer Levy. Pick-a-pic: An open dataset of user preferences for text-to-image generation. *Advances in neural information processing systems*, 36:36652–36663, 2023. 1, 2, 5, 6
- [31] Weijie Kong, Qi Tian, Zijian Zhang, Rox Min, Zuozhuo Dai, Jin Zhou, Jiangfeng Xiong, Xin Li, Bo Wu, Jianwei Zhang, et al. Hunyuanvideo: A systematic framework for large video generative models. *arXiv preprint arXiv:2412.03603*, 2024. 1, 3
- [32] Kimin Lee, Hao Liu, Moonkyung Ryu, Olivia Watkins, Yuqing Du, Craig Boutilier, Pieter Abbeel, Mohammad Ghavamzadeh, and Shixiang Shane Gu. Aligning text-to-image models using human feedback. *arXiv preprint arXiv:2302.12192*, 2023. 2
- [33] Tony Lee, Michihiro Yasunaga, Chenlin Meng, Yifan Mai, Joon Sung Park, Agrim Gupta, Yunzhi Zhang, Deepak Narayanan, Hannah Teufel, Marco Bellagente, et al. Holistic evaluation of text-to-image models. *Advances in Neural Information Processing Systems*, 36:69981–70011, 2023. 2
- [34] Zhanhao Liang, Yuhui Yuan, Shuyang Gu, Bohan Chen, Tiankai Hang, Mingxi Cheng, Ji Li, and Liang Zheng. Aesthetic post-training diffusion models from generic preferences with step-by-step preference optimization. In *Proceedings of the Computer Vision and Pattern Recognition Conference*, pages 13199–13208, 2025. 2
- [35] Yaron Lipman, Ricky TQ Chen, Heli Ben-Hamu, Maximilian Nickel, and Matt Le. Flow matching for generative modeling. *arXiv preprint arXiv:2210.02747*, 2022. 3
- [36] Jie Liu, Gongye Liu, Jiajun Liang, Yangguang Li, Jiaheng Liu, Xintao Wang, Pengfei Wan, Di Zhang, and Wanli Ouyang. Flow-grpo: Training flow matching models via online rl, 2025. URL <https://arxiv.org/abs/2505.05470>. 1, 2
- [37] Jie Liu, Gongye Liu, Jiajun Liang, Yangguang Li, Jiaheng Liu, Xintao Wang, Pengfei Wan, Di Zhang, and Wanli Ouyang. Flow-grpo: Training flow matching models via online rl. *arXiv preprint arXiv:2505.05470*, 2025. 2, 4, 5, 6, 7
- [38] Jie Liu, Gongye Liu, Jiajun Liang, Ziyang Yuan, Xiaokun Liu, Mingwu Zheng, Xiele Wu, Qiulin Wang, Menghan Xia, Xintao Wang, et al. Improving video generation with human feedback. *arXiv preprint arXiv:2501.13918*, 2025. 2
- [39] Runtao Liu, Haoyu Wu, Ziqiang Zheng, Chen Wei, Yingqing He, Renjie Pi, and Qifeng Chen. Videopo: Omni-preference alignment for video diffusion generation. In *Proceedings of the Computer Vision and Pattern Recognition Conference*, pages 8009–8019, 2025. 2
- [40] Xingchao Liu, Chengyue Gong, and Qiang Liu. Flow straight and fast: Learning to generate and transfer data with rectified flow. *arXiv preprint arXiv:2209.03003*, 2022. 3
- [41] Ilya Loshchilov and Frank Hutter. Decoupled weight decay regularization. *arXiv preprint arXiv:1711.05101*, 2017. 5
- [42] Zhuoyan Luo, Fengyuan Shi, Yixiao Ge, Yujiu Yang, Limin Wang, and Ying Shan. Open-magvit2: An open-source project toward democratizing auto-regressive visual generation. *arXiv preprint arXiv:2409.04410*, 2024. 2
- [43] Sourab Mangrulkar, Sylvain Gugger, Lysandre Debut, Younes Belkada, Sayak Paul, and Benjamin Bossan. PEFT: State-of-the-art parameter-efficient fine-tuning methods. <https://github.com/huggingface/peft>, 2022. 5
- [44] Zichen Miao, Jiang Wang, Ze Wang, Zhengyuan Yang, Lijuan Wang, Qiang Qiu, and Zicheng Liu. Training diffusion models towards diverse image generation with reinforcement learning. In *Proceedings of the IEEE/CVF Conference on Computer Vision and Pattern Recognition*, pages 10844–10853, 2024. 2
- [45] OpenAI. Hello gpt-4o, 2024. 5
- [46] William Peebles and Saining Xie. Scalable diffusion models with transformers. In *Proceedings of the IEEE/CVF international conference on computer vision*, pages 4195–4205, 2023. 1, 2
- [47] Xue Bin Peng, Aviral Kumar, Grace Zhang, and Sergey Levine. Advantage-weighted regression: Simple and scalable off-policy reinforcement learning. *arXiv preprint arXiv:1910.00177*, 2019. 2
- [48] Dustin Podell, Zion English, Kyle Lacey, Andreas Blattmann, Tim Dockhorn, Jonas Müller, Joe Penna, and

- Robin Rombach. Sdxl: Improving latent diffusion models for high-resolution image synthesis. *arXiv preprint arXiv:2307.01952*, 2023. 1, 2
- [49] Gabriel Poesia, David Broman, Nick Haber, and Noah Goodman. Learning formal mathematics from intrinsic motivation. *Advances in Neural Information Processing Systems*, 37:43032–43057, 2024. 3
- [50] Ben Poole, Ajay Jain, Jonathan T Barron, and Ben Mildenhall. Dreamfusion: Text-to-3d using 2d diffusion. *arXiv preprint arXiv:2209.14988*, 2022. 1, 2, 3
- [51] Mihir Prabhudesai, Anirudh Goyal, Deepak Pathak, and Katerina Fragkiadaki. Aligning text-to-image diffusion models with reward backpropagation. 2023. 2
- [52] Mihir Prabhudesai, Russell Mendonca, Zheyang Qin, Katerina Fragkiadaki, and Deepak Pathak. Video diffusion alignment via reward gradients. *arXiv preprint arXiv:2407.08737*, 2024. 2
- [53] Alec Radford, Jong Wook Kim, Chris Hallacy, Aditya Ramesh, Gabriel Goh, Sandhini Agarwal, Girish Sastry, Amanda Askell, Pamela Mishkin, Jack Clark, et al. Learning transferable visual models from natural language supervision. In *International conference on machine learning*, pages 8748–8763. PmLR, 2021. 2, 5, 6
- [54] Rafael Rafailov, Archit Sharma, Eric Mitchell, Christopher D Manning, Stefano Ermon, and Chelsea Finn. Direct preference optimization: Your language model is secretly a reward model. *Advances in neural information processing systems*, 36:53728–53741, 2023. 2
- [55] Robin Rombach, Andreas Blattmann, Dominik Lorenz, Patrick Esser, and Björn Ommer. High-resolution image synthesis with latent diffusion models. In *Proceedings of the IEEE/CVF conference on computer vision and pattern recognition*, pages 10684–10695, 2022. 1, 2
- [56] Chitwan Saharia, William Chan, Saurabh Saxena, Lala Li, Jay Whang, Emily L Denton, Kamyar Ghasemipour, Raphael Gontijo Lopes, Burcu Karagol Ayan, Tim Salimans, et al. Photorealistic text-to-image diffusion models with deep language understanding. *Advances in neural information processing systems*, 35:36479–36494, 2022. 1, 2, 5, 6, 7
- [57] Christoph Schuhmann, Romain Beaumont, Richard Vencu, Cade Gordon, Ross Wightman, Mehdi Cherti, Theo Coombes, Aarush Katta, Clayton Mullis, Mitchell Wortsman, et al. Laion-5b: An open large-scale dataset for training next generation image-text models. *Advances in neural information processing systems*, 35:25278–25294, 2022. 5
- [58] John Schulman, Filip Wolski, Prafulla Dhariwal, Alec Radford, and Oleg Klimov. Proximal policy optimization algorithms. *arXiv preprint arXiv:1707.06347*, 2017. 2
- [59] Zhihong Shao, Peiyi Wang, Qihao Zhu, Runxin Xu, Junxiao Song, Xiao Bi, Haowei Zhang, Mingchuan Zhang, YK Li, Yang Wu, et al. Deepseekmath: Pushing the limits of mathematical reasoning in open language models. *arXiv preprint arXiv:2402.03300*, 2024. 2, 3, 4
- [60] Shelly Sheynin, Adam Polyak, Uriel Singer, Yuval Kirstain, Amit Zohar, Oron Ashual, Devi Parikh, and Yaniv Taigman. Emu edit: Precise image editing via recognition and generation tasks. In *Proceedings of the IEEE/CVF Conference on Computer Vision and Pattern Recognition*, pages 8871–8879, 2024. 1
- [61] Yichun Shi, Peng Wang, Jianglong Ye, Mai Long, Kejie Li, and Xiao Yang. Mvdream: Multi-view diffusion for 3d generation. *arXiv preprint arXiv:2308.16512*, 2023. 1, 2, 3
- [62] Yichun Shi, Peng Wang, and Weilin Huang. Seedit: Align image re-generation to image editing. *arXiv preprint arXiv:2411.06686*, 2024. 1
- [63] Inkyu Shin, Chenglin Yang, and Liang-Chieh Chen. Deeply supervised flow-based generative models. *arXiv preprint arXiv:2503.14494*, 2025. 2
- [64] Joonghyuk Shin, Minguk Kang, and Jaesik Park. Fill-up: Balancing long-tailed data with generative models. *arXiv preprint arXiv:2306.07200*, 2023. 1
- [65] Uriel Singer, Shelly Sheynin, Adam Polyak, Oron Ashual, Iurii Makarov, Filippos Kokkinos, Naman Goyal, Andrea Vedaldi, Devi Parikh, Justin Johnson, et al. Text-to-4d dynamic scene generation. *arXiv preprint arXiv:2301.11280*, 2023. 1
- [66] Yang Song, Jascha Sohl-Dickstein, Diederik P Kingma, Abhishek Kumar, Stefano Ermon, and Ben Poole. Score-based generative modeling through stochastic differential equations. *arXiv preprint arXiv:2011.13456*, 2020. 3
- [67] Kaiyue Sun, Kaiyi Huang, Xian Liu, Yue Wu, Zihan Xu, Zhenguo Li, and Xihui Liu. T2v-compbench: A comprehensive benchmark for compositional text-to-video generation. In *Proceedings of the Computer Vision and Pattern Recognition Conference*, pages 8406–8416, 2025. 2
- [68] Peize Sun, Yi Jiang, Shoufa Chen, Shilong Zhang, Bingyue Peng, Ping Luo, and Zehuan Yuan. Autoregressive model beats diffusion: Llama for scalable image generation. *arXiv preprint arXiv:2406.06525*, 2024. 2
- [69] Bram Wallace, Meihua Dang, Rafael Rafailov, Linqi Zhou, Aaron Lou, Senthil Purushwalkam, Stefano Ermon, Caiming Xiong, Shafiq Joty, and Nikhil Naik. Diffusion model alignment using direct preference optimization. In *Proceedings of the IEEE/CVF Conference on Computer Vision and Pattern Recognition*, pages 8228–8238, 2024. 1, 2
- [70] Team Wan, Ang Wang, Baole Ai, Bin Wen, Chaojie Mao, Chen-Wei Xie, Di Chen, Feiwu Yu, Haiming Zhao, Jianxiao Yang, et al. Wan: Open and advanced large-scale video generative models. *arXiv preprint arXiv:2503.20314*, 2025. 1, 3
- [71] Juniu Wang, Hangjie Yuan, Dayou Chen, Yingya Zhang, Xiang Wang, and Shiwei Zhang. Modelscope text-to-video technical report. *arXiv preprint arXiv:2308.06571*, 2023. 1
- [72] Yibin Wang, Yuhang Zang, Hao Li, Cheng Jin, and Jiaqi Wang. Unified reward model for multimodal understanding and generation. *arXiv preprint arXiv:2503.05236*, 2025. 2, 5, 6
- [73] Yinong Oliver Wang, Younjoon Chung, Chen Henry Wu, and Fernando De la Torre. Domain gap embeddings for generative dataset augmentation. In *Proceedings of the IEEE/CVF Conference on Computer Vision and Pattern Recognition*, pages 28684–28694, 2024. 1
- [74] Zhengyi Wang, Cheng Lu, Yikai Wang, Fan Bao, Chongxuan Li, Hang Su, and Jun Zhu. Prolificdreamer: High-fidelity and

- diverse text-to-3d generation with variational score distillation. *Advances in neural information processing systems*, 36: 8406–8441, 2023. 1, 2
- [75] Xiaoshi Wu, Yiming Hao, Keqiang Sun, Yixiong Chen, Feng Zhu, Rui Zhao, and Hongsheng Li. Human preference score v2: A solid benchmark for evaluating human preferences of text-to-image synthesis. *arXiv preprint arXiv:2306.09341*, 2023. 1, 2, 5, 6
- [76] Shitao Xiao, Yueze Wang, Junjie Zhou, Huaying Yuan, Xin-grun Xing, Ruiran Yan, Chaofan Li, Shuting Wang, Tiejun Huang, and Zheng Liu. Omnigen: Unified image generation. In *Proceedings of the Computer Vision and Pattern Recognition Conference*, pages 13294–13304, 2025. 1
- [77] Fangzhi Xu, Hang Yan, Chang Ma, Haiteng Zhao, Qiushi Sun, Kanzhi Cheng, Junxian He, Jun Liu, and Zhiyong Wu. Genius: A generalizable and purely unsupervised self-training framework for advanced reasoning. *arXiv preprint arXiv:2504.08672*, 2025. 3
- [78] Jiazhen Xu, Xiao Liu, Yuchen Wu, Yuxuan Tong, Qinkai Li, Ming Ding, Jie Tang, and Yuxiao Dong. Imagereward: Learning and evaluating human preferences for text-to-image generation. *Advances in Neural Information Processing Systems*, 36:15903–15935, 2023. 1, 2, 5, 6
- [79] Kai Yang, Jian Tao, Jiafei Lyu, Chunjiang Ge, Jiabin Chen, Weihang Shen, Xiaolong Zhu, and Xiu Li. Using human feedback to fine-tune diffusion models without any reward model. In *Proceedings of the IEEE/CVF Conference on Computer Vision and Pattern Recognition*, pages 8941–8951, 2024. 2
- [80] Zuhao Yang, Fangneng Zhan, Kunhao Liu, Muyu Xu, and Shijian Lu. Ai-generated images as data source: The dawn of synthetic era. *arXiv preprint arXiv:2310.01830*, 2023. 1
- [81] Jiahui Yu, Yuanzhong Xu, Jing Yu Koh, Thang Luong, Gungjan Baid, Zirui Wang, Vijay Vasudevan, Alexander Ku, Yinfei Yang, Burcu Karagol Ayan, et al. Scaling autoregressive models for content-rich text-to-image generation. *arXiv preprint arXiv:2206.10789*, 2(3):5, 2022. 2, 6
- [82] Qihang Yu, Mark Weber, Xueqing Deng, Xiaohui Shen, Daniel Cremers, and Liang-Chieh Chen. An image is worth 32 tokens for reconstruction and generation. *Advances in Neural Information Processing Systems*, 37:128940–128966, 2024. 2
- [83] Huizhuo Yuan, Zixiang Chen, Kaixuan Ji, and Quanquan Gu. Self-play fine-tuning of diffusion models for text-to-image generation. *Advances in Neural Information Processing Systems*, 37:73366–73398, 2024. 2
- [84] Weizhe Yuan, Richard Yuanzhe Pang, Kyunghyun Cho, Xian Li, Sainbayar Sukhbaatar, Jing Xu, and Jason E Weston. Self-rewarding language models. In *Forty-first International Conference on Machine Learning*, 2024. 3
- [85] Eric Zelikman, Yuhuai Wu, Jesse Mu, and Noah Goodman. Star: Bootstrapping reasoning with reasoning. *Advances in Neural Information Processing Systems*, 35:15476–15488, 2022. 3
- [86] Jiacheng Zhang, Jie Wu, Weifeng Chen, Yatai Ji, Xuefeng Xiao, Weilin Huang, and Kai Han. Onlinevpo: Align video diffusion model with online video-centric preference optimization. *arXiv preprint arXiv:2412.15159*, 2024. 2
- [87] Zechuan Zhang, Ji Xie, Yu Lu, Zongxin Yang, and Yi Yang. In-context edit: Enabling instructional image editing with in-context generation in large scale diffusion transformer. *arXiv preprint arXiv:2504.20690*, 2025. 1
- [88] Andrew Zhao, Yiran Wu, Yang Yue, Tong Wu, Quentin Xu, Matthieu Lin, Shenzi Wang, Qingyun Wu, Zilong Zheng, and Gao Huang. Absolute zero: Reinforced self-play reasoning with zero data. *arXiv preprint arXiv:2505.03335*, 2025. 3
- [89] Hanyang Zhao, Haoxian Chen, Ji Zhang, David D Yao, and Wenpin Tang. Score as action: Fine-tuning diffusion generative models by continuous-time reinforcement learning. *arXiv preprint arXiv:2502.01819*, 2025. 2
- [90] Xuandong Zhao, Zhewei Kang, Aosong Feng, Sergey Levine, and Dawn Song. Learning to reason without external rewards. *arXiv preprint arXiv:2505.19590*, 2025. 3
- [91] Kaiwen Zheng, Huayu Chen, Haotian Ye, Haoxiang Wang, Qinsheng Zhang, Kai Jiang, Hang Su, Stefano Ermon, Jun Zhu, and Ming-Yu Liu. Diffusionnft: Online diffusion reinforcement with forward process. *arXiv preprint arXiv:2509.16117*, 2025. 2
- [92] Daquan Zhou, Weimin Wang, Hanshu Yan, Weiwei Lv, Yizhe Zhu, and Jiashi Feng. Magicvideo: Efficient video generation with latent diffusion models. *arXiv preprint arXiv:2211.11018*, 2022. 1
- [93] Yuxin Zuo, Kaiyan Zhang, Li Sheng, Shang Qu, Ganqu Cui, Xuekai Zhu, Haozhan Li, Yuchen Zhang, Xinwei Long, Ermo Hua, et al. Ttrl: Test-time reinforcement learning. *arXiv preprint arXiv:2504.16084*, 2025. 3

Improving Text-to-Image Generation with Intrinsic Self-Confidence Rewards

Supplementary Material

Supplementary Contents

- Rationale of SOLACE
- SOLACE Post-Training on SD3.5-L
- Applying SOLACE on FLUX.1-Dev
- Training Collapse Analysis
- Additional ablation studies
- Additional Implementation Details
- User Study Instructions and Interface
- Additional Qualitative Results

7. Rationale of SOLACE

We motivate SOLACE by testing whether a model’s *denoising-based self-confidence* correlates with perceived image quality when generation settings are made progressively stronger while keeping the underlying model fixed. Specifically, we compare three inference regimes for the same text-to-image model: (i) 10 sampling steps without CFG, (ii) 10 steps with CFG, and (iii) 20 steps with CFG in Fig. 6. For each regime, we compute the self-confidence score defined in Sec. 4.1 on the model’s own outputs (same scorer and parameters across all cases). Empirically, the self-confidence distribution increases from (i) to (ii) to (iii), matching the observed rise in visual fidelity and prompt adherence. Because the signal is computed post hoc by the *same* model regardless of guidance or step count, these trends are not artifacts of an external evaluator; rather, they indicate that better samples are also easier for the model to self-denoise. This observation provides the rationale for treating denoising-based self-confidence as a model-native reward for post-training.

8. SOLACE Post-Training on SD3.5-L

To assess scalability, we apply SOLACE to SD3.5-L [16], a larger base model than the SD3.5-M used in the main experiments. Unless otherwise noted, we reuse the same training recipe (shortened denoising horizon, suffix-only updates, shared probes, CFG-free scoring). As reported in Tab. 3, SOLACE yields *consistent gains* in compositional generation, text rendering, and text-image alignment, while remaining competitive on human-preference metrics (e.g., HPSv2, PickScore). These results suggest that SOLACE scales to higher-capacity text-to-image models without inducing reward hacking and remains effective beyond the SD3.5-M setting.

9. Applying SOLACE on FLUX.1-Dev

To test architectural generality, we apply SOLACE to **FLUX.1-Dev** [3], a flow-matching text-to-image generator with a design distinct from SD3.5. We keep the core SOLACE recipe unchanged (shortened denoising horizon, suffix-only updates, shared probes, CFG-free scoring), adapting only to the model’s native scheduler and inference step count. A small deviation is the suffix window: we set $\rho = 0.5$, i.e., train on the latter half of the scheduler steps, which increased training stability in this setting. As

“A road sign near a cliff warns “Steep Drop” with a prominent skull icon, set against a dramatic, foggy backdrop that emphasizes the danger and isolation of the location.”



A bustling supermarket aisle with a clear sign reading “Baking Supplies Section”, featuring shelves stocked with flour, sugar, and spices. Shoppers are browsing, and the lighting highlights the vibrant packaging of baking ingredients.



Sampling steps: 10 CFG: Disabled Mean Self-Confidence: 0.3147	Sampling steps: 10 CFG: Enabled Mean Self-Confidence: 0.5157	Sampling steps: 20 CFG: Enabled Mean Self-Confidence: 0.9773
---	--	--

Figure 6. **Rationale of SOLACE.** Distributions of the denoising-based self-confidence under three inference settings—10 steps (no CFG), 10 steps (CFG), and 20 steps (CFG). The distribution shifts monotonically rightward (higher self-confidence) in the same order that visual quality improves, indicating that the ability to recover injected noise is predictive of sample quality even when the scorer is the same model. This alignment underpins SOLACE’s use of self-confidence as an intrinsic reward.

reported in Tab. 3, SOLACE delivers *consistent gains* in compositional generation, text rendering, and text-image alignment, while remaining competitive on human-preference metrics (e.g., HPSv2, PickScore). The results indicate that SOLACE transfers effectively across architectures and remains robust on another representative flow-matching T2I model.

10. Training Collapse Analysis

When and why collapse occurs. We monitor the batch-mean self-confidence (negative log error, averaged over probes and probed timesteps) across training iterations. Collapse is characterized by a rapid, sustained surge in this score—an overconfidence spike—followed by degenerate, low-texture generations (reward hacking). Empirically, two settings precipitate this behavior: (i) training on too many timesteps ($\rho > 0.6$ in $|\mathcal{T}_{\text{train}}| = \lceil \rho |\mathcal{T}| \rceil$), which exposes early, easily exploitable steps; and (ii) sampling the G rollout candidates *without* CFG, which reduces exploration and inflates apparent self-confidence. A KL anchor alone is insufficient to prevent these modes.

Mitigations used in SOLACE. We restrict training to the latter 60% of steps ($\rho = 0.6$), keep CFG *on* during rollouts (but *off* when scoring self-confidence), and retain clipping, per-timestep

	Task-specific		Image Quality		Human Preference			
	GenEval	OCR	ClipScore	Aesthetic	PickScore	HPSv2.1	ImageReward	UnifiedReward
SD3.5-M (2.5B)	0.65	0.61	0.282	5.36	22.34	0.279	0.84	3.08
+ SOLACE (Ours)	0.71	0.67	0.288	5.39	22.41	0.278	0.87	3.11
SD3.5-L† (8.1B)	0.71	0.68	0.289	5.50	22.91	0.288	0.96	3.25
(Reproduced)	0.51	0.68	0.284	5.28	21.86	0.264	0.70	2.98
†+ SOLACE (Ours)	0.58	0.74	0.288	5.25	21.91	0.253	0.65	2.98
FLUX.1-Dev† (12B)	0.66	0.59	0.295	5.71	22.69	0.292	0.96	3.27
(Reproduced)	0.66	0.61	0.269	5.71	22.84	0.274	0.88	3.21
+ SOLACE (Ours)	0.66	0.65	0.271	5.67	22.69	0.292	0.90	3.23

Table 3. **Applying SOLACE to SD3.5-L [16] and FLUX.1-Dev [3].** We apply SOLACE on additional models of SD3.5-L and FLUX.1-Dev, to verify the effect of SOLACE given (1) a larger base model, and (2) a different architecture from SD3.5-M. † denotes results taken from DiffusionNFT [91]. We base our experiments on our reproduced results based on the official weights of SD3.5-L [16] and FLUX.1-Dev [3]. The results show that SOLACE consistently results in improved compositionality, text rendering and text-image alignment, while being competitive at human preference metrics.

weighting, and antithetic probes. These choices suppress overconfidence spikes and stabilize learning.

11. Additional Ablation Studies

We conduct additional ablation studies and comparative experiments to validate the design choices of SOLACE. The results are summarized in Tab. 5.

11.1. Caption datasets for SOLACE

SOLACE relies on intrinsic self-confidence and thus requires only prompts (not external reward models). We compare three prompt sources: (i) *text-rendering* (OCR) prompts from Flow-GRPO [37] (our default), (ii) *PickScore* [30] prompts, and (iii) *GenEval* [21] prompts. As shown in Tab. 3, denser, more prescriptive prompts (OCR) yield the strongest gains; empirically, self-confidence is most reliable when the text condition is explicit and descriptive. We provide the descriptions and examples for each prompt dataset in Tab. 4.

11.2. Effect of group size

We clarify a typographical error in the main paper: although we stated $G=24$, all experiments used $G=16$. Varying G shows that $G=16$ outperforms $G=8$ (more within-prompt exploration improves group-relative normalization) while $G=32$ destabilizes training: larger groups reduce the number of distinct prompts per batch, lowering inter-prompt diversity and increasing the risk of over-optimization under relative advantages. In practice, $G=16$ strikes a robust compute–stability trade-off.

11.3. Stepwise vs. aggregated reward

Although SOLACE’s self-confidence can be computed per step, we find that using the *aggregated* reward, *i.e.*, averaging weighted per-step scores over the probed timesteps, consistently performs better than optimizing stepwise advantages. Stepwise improvements at individual timesteps need not translate to a better final sample and tend to increase variance and solver sensitivity; ag-

gregation provides a more stable, outcome-aligned signal for post-training.

12. Additional Implementation Details

In this section we summarize the main implementation choices used in our SOLACE training pipeline. **We acknowledge and correct a typographical error in the main paper:** although we stated that the group size was $G = 24$, all experiments were in fact conducted with $G = 16$. The summary of hyperparameterse and configurations is illustrated in Tab. 6.

12.1. Base models and LoRA configuration

We build on the `StableDiffusion3Pipeline` from `diffusers` with the pretrained model `SD3.5-M: stabilityai/stable-diffusion-3.5-medium`. We freeze all components except the denoiser: the VAE and all text encoders are kept fixed and used only for inference. Only the main transformer (UNet-like denoiser) is updated during training, based on LoRA. We run the text encoders in mixed precision (`fp16` in our main SOLACE runs) and keep the VAE in `fp32` for stability.

For parameter-efficient fine-tuning we apply LoRA to the transformer with

- LoRA rank $r = 32$ and scaling factor $\alpha = 64$,
- Gaussian initialization of LoRA weights,
- Target modules inside each attention block:

```
attn.add_k_proj, attn.add_q_proj,
attn.add_v_proj, attn.to_add_out,
attn.to_k, attn.to_q, attn.to_v, attn.to_out.0.
```

All non-LoRA base weights remain frozen.

12.2. Datasets and prompt processing

We consider two kinds of prompt datasets:

- **Plain text prompt datasets.** We store the prompts in plain text files `train.txt` and `test.txt`. Each line contains a single prompt string. (*e.g.* `PickScore`, `Text Rendering` dataset)

(i) Text-rendering (OCR) prompts — default

<i>Characteristics</i>	Dense, explicit textual content (exact strings, font/placement hints), strong conditioning for legibility and alignment.
<i>Examples</i>	“A postage stamp design featuring the motto ”Unity in Diversity”, showcasing a vibrant collage of people from various ethnic backgrounds, each holding hands in a circle, set against a backdrop of colorful, interwoven patterns symbolizing unity and cultural richness.” “In a luxurious hotel lobby, an elegant digital display above the elevator reads ”Now Playing”. Soft, ambient elevator music fills the space, enhancing the serene and welcoming atmosphere. A plush, modern sofa and a glass coffee table are seen in the foreground, with polished marble floors reflecting the ambient light.” “A sleek, modern corporate lobby featuring a large, minimalist sculpture prominently inscribed with ”Innovate or Perish”, reflecting the company’s commitment to forward-thinking. The sculpture stands against a backdrop of glass and steel, with subtle lighting enhancing its form and the powerful message it conveys.”

(ii) PickScore prompts

<i>Characteristics</i>	Open-ended statements; often adds context with simple concatenation of adjectives; weaker constraints on text content/layout.
<i>Examples</i>	“An attractive young woman petting a cat” “(a girl in steampunk fantasy world), (ultra detailed prosthetic arm and leg), (beautifully drawn face:1.2), blueprints, (magic potions:1.4), mechanical tools, plants, (a small cat:1.1), silver hair, (full body:1.2), magic dust, books BREAK (complex ultra detailed of medieval fantasy city), (steampunk fantasy:1.2), indoors, workshop, (Steam-powered machines:1.2), (clockwork automatons:1.2), (a small wooden toy), (intricate details:1.6), lamps, colorful details, iridescent colors, BREAK illustration, ((masterpiece:1.2, best quality)), 4k, ultra detailed, solo, (photorealistic:1.2), asymmetry, looking at viewer, smile” “Cyborg cow, cyberpunk alien india, body painting, bull, star wars design, third eye, mehendi body art, yantra, cyberpunk mask, baroque style, dark fantasy, kathakali characters, high tech, detailed, spotlight, shadow color, high contrast, cyberpunk city, neon light, colorful, bright, high tech, high contrast, synthesized body, hyper realistic, 8k, epic ambient light, octane rendering, kathakali, soft ambient light, HD,”

(iii) GenEval prompts

<i>Characteristics</i>	Compositional verification (objects, counts, relations), moderate specificity, minimal typography.
<i>Examples</i>	“a photo of a yellow bus and an orange handbag” “a photo of four surfboards” “a photo of a book left of a cat”

Table 4. **Prompt sources compared for SOLACE.** Denser, text-focused prompts (OCR) provide stronger supervision signals for intrinsic self-confidence, leading to larger gains than more open-ended (PickScore) or simple compositional (GenEval) prompts.

• **GenEval-style metadata.** For experiments on GenEval-style prompts we use JSONL files `{train,test}.metadata.jsonl`, where each line is a JSON object that contains at least a "prompt" field and additional metadata.

For each batch of prompts we compute text embeddings using the three SD3.5 text encoders. We also precompute embeddings for the empty prompt "" and use them as unconditional embeddings for classifier-free guidance (CFG) during sampling and log-probability computation.

12.3. Distributed sampling and grouping

We use HuggingFace Accelerate [23] for distributed training. Let N be the number of GPUs (processes), and let B_{sample} denote the per-device sample batch size. In our main SOLACE setting we use $N = 8, B_{\text{sample}} = 8, G = 16$. Thus a single sampling batch contains $N B_{\text{sample}} = 64$ images, corresponding to $64/16 = 4$ distinct prompts, each with $G = 16$ candidate images. We train for 2,000 iterations, which takes around 30 hours on $8 \times \text{NVIDIA 332 RTX PRO 6000 Blackwell GPUs}$.

12.4. KL regularization

Following Flow-GRPO, regularize the policy via a KL term that constrains the transition mean to stay close to a reference (the base model without LoRA):

- The SDE step module returns the current mean μ_θ and a reference variance σ_t^2 .
- We compute a reference mean μ_{ref} by temporarily disabling LoRA adapters and re-evaluating the same step.
- Assuming Gaussian transitions with equal variance, the per-step KL divergence simplifies to

$$D_{\text{KL}} = \frac{1}{2\sigma_t^2} \|\mu_\theta - \mu_{\text{ref}}\|_2^2.$$

We average this KL over spatial dimensions and the batch and add it to the policy loss with weight $\beta = 0.04$.

13. User Study Instructions and Interface

We provide the details of the instructions and interface used for the user study.

	Task-specific		Image Quality		Human Preference			
	GenEval	OCR	ClipScore	Aesthetic	PickScore	HPSv2.1	ImageReward	UnifiedReward
<i>Caption dataset used for SOLACE</i>								
-	0.65	0.61	0.282	5.36	22.34	0.279	0.84	3.08
PickScore prompts	0.70	0.62	0.285	5.26	22.13	0.278	0.65	2.96
GenEval prompts	0.71	0.62	0.286	5.32	22.35	0.275	0.80	3.05
OCR prompts (Ours)	0.71	0.67	0.288	5.39	22.41	0.278	0.87	3.11
<i>Group size G</i>								
8	0.70	0.64	0.285	5.29	22.28	0.267	0.75	3.00
16 (Ours)	0.71	0.67	0.288	5.39	22.41	0.278	0.87	3.11
32	0.61	0.51	0.274	5.18	21.73	0.226	0.16	2.73
<i>Step-wise reward vs. Aggregated reward</i>								
Stepwise	0.67	0.60	0.285	5.39	22.36	0.277	0.83	3.07
Aggregated (Ours)	0.71	0.67	0.288	5.39	22.41	0.278	0.87	3.11

Table 5. **Additional ablation/comparative results.** The results show that our current design choices for the (1) Caption dataset used, (2) Group size G , and (3) Aggregated self-confidence rewards yield the best performances.

Instructions. For each text prompt, you will be shown a pair of *AI-generated* images (left and right). For every image pair, you are asked to answer the following two questions *independently*:

1. **Visual realism and appeal:** Which image do you find to be more visually realistic and appealing?
2. **Text-image alignment:** Which image better aligns with the given text description?

For each question, please select your preferred image (left or right) based solely on the specified criterion.

Interface. The user interface used in the study is illustrated in Fig. 8.

14. Additional Qualitative Results

We provide side-by-side samples for (i) PickScore–post-trained (Flow-GRPO) SD3.5–M, (ii) FLUX.1–Dev, and (iii) SD3.5–L in Fig. 9. Across diverse prompts, SOLACE yields visibly sharper text rendering, more faithful object counts and relations, and fewer artifacts, echoing the quantitative gains in compositionality, text rendering, and text–image alignment, with no obvious regressions on non-target aspects.

Category	Hyperparameter	Value (SOLACE, SD3.5-M)
Model	Base model	stabilityai/stable-diffusion-3.5-medium (SD3.5-M)
	Components trained	Transformer (denoiser) only; VAE and all text encoders frozen
LoRA	LoRA usage	use_lora = True
	Rank r	32
	Scaling factor α	64
	Init of LoRA weights	Gaussian
	Target modules	attn.add_k_proj, attn.add_q_proj, attn.add_v_proj, attn.to_add_out, attn.to_k, attn.to_q, attn.to_v, attn.to_out.0
Data / prompts	Train / test files	train.txt, test.txt (one prompt per line)
	Tokenization	SD3.5 tokenizers; max length 128 (embeddings), 256 (logging)
Sampling	Image resolution	512×512
	Sampler steps (train / eval)	train:10, eval:40
	Train timestep fraction	train.timestep_fraction = 0.99 $\Rightarrow T_{\text{train}} = 9$
	Suffix proportion ρ in GRPO	0.6
	Guidance scale (train/eval)	sample.guidance_scale = 4.5
	Noise level (SDE step)	sample.noise_level = 0.7
	Train batch size / GPU (sampling)	sample.train_batch_size = 8 images
	Test batch size / GPU	sample.test_batch_size = 16 images
	Images per prompt (group size G)	sample.num_image_per_prompt = 16
	Number of GPUs	8
	Batches per epoch (sampling)	sample.num_batches_per_epoch = 4
	Global samples / batch	8 (bs) \times 8 (GPUs) = 64 images
	Prompts / batch	64/16 = 4 prompts per sampling batch
Same latent per prompt	sample.same_latent = False	
Self-confidence (SOLACE)	Probes per step K	8 (antithetic pairing: $K/2$ noise, $K/2$ negated)
	Probe timesteps	Last half of used timesteps: $j = 4, \dots, 8$ (for $T_{\text{train}} = 9$)
	Noise schedule for probe	$\lambda_t = \tau_t/1000$; $x_t = (1 - \lambda_t)x_0 + \lambda_t\epsilon$
	Per-step score	$s_t = -\log(\text{MSE}_t + 10^{-6})$, MSE between injected and predicted noise
	Normalization	Per-timestep batch-wise z-score, then mean over timesteps
	CFG inside probe	Disabled (conditional branch only)
Training (GRPO)	PPO / GRPO clip range	$\rho_{i,t}$ clipped to $[1 - \text{clip_range}, 1 + \text{clip_range}]$ (PPO style)
	KL regularizer weight	train.beta = 0.04
	KL form	$D_{\text{KL}} = \ \mu_\theta - \mu_{\text{ref}}\ _2^2 / (2\sigma_t^2)$ (mean-only Gaussian)
Optimization / EMA	Optimizer	AdamW on LoRA parameters (no base-parameter updates)
	Learning rate	3×10^{-4} (constant)
	Gradient clipping	Global norm clipping at train.max_grad_norm
	EMA usage	train.ema = True
	EMA decay	0.9
	EMA update interval	Every 8 optimizer steps (update_step_interval = 8)
	EMA usage in eval	EMA weights used for evaluation; online weights restored afterwards
External rewards / eval	Training reward	Internal self-confidence only (no external reward in training)
	SDS-only eval	Optional SDS self-confidence evaluation on EMA model for monitoring

Table 6. Hyperparameters and key implementation details for SOLACE training on SD3.5-M.



Figure 7. **Visualization of training collapse in SOLACE.** Self-confidence (y-axis) versus training iteration under different settings. Using $\rho > 0.6$ or sampling rollouts without CFG drives a steep, short-horizon increase in self-confidence, followed by degenerate outputs—evidence of reward hacking. SOLACE’s default settings ($\rho=0.6$ and CFG for rollouts) avoid this behavior while preserving steady improvements.

A bird and its reflection in a fountain



Which image is more visually realistic and appealing?

- Left
- Right
- Same

Which image better aligns with the text description?

- Left
- Right
- Same

Figure 8. User study interface used to collect human preferences between pairs of AI-generated images.

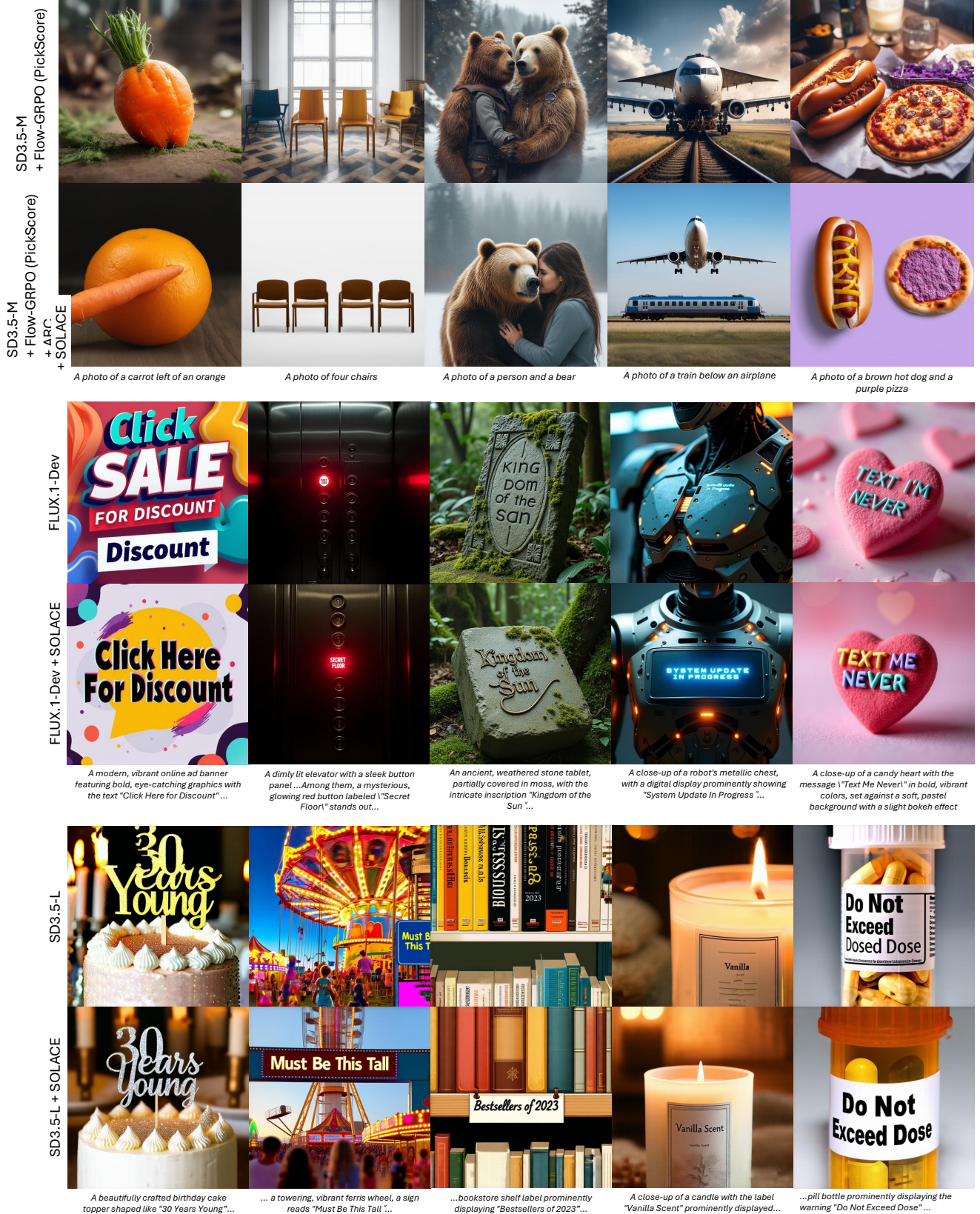


Figure 9. **Additional qualitative results of SOLACE.** We present additional qualitative results of SOLACE when applied to (1) Flow-GRPO [37] post-trained SD3.5-M [16], (2) FLUX.1-Dev [3], and (3) SD3.5-L [16]. Best viewed on electronics.